The 4th International Symposium - Supercritical CO_2 Power Cycles
September 9-10, 2014, Pittsburgh, Pennsylvania

THE EFFECT OF TEMPERATURE ON THE sCO_2 COMPATIBILITY OF CONVENTIONAL STRUCTURAL ALLOYS

Bruce A. Pint
Group Leader
Oak Ridge National Laboratory
Oak Ridge, TN 37831-6156 USA
pintba@ornl.gov

James R. Keiser
Distinguished R&D Staff Member
Oak Ridge National Laboratory
Oak Ridge, TN 37831-6156 USA
keiserjr@ornl.gov

Bruce Pint is the Group Leader of the Corrosion Science & Technology Group in the Materials Science & Technology Division at ORNL. He received his Ph.D. from M.I.T. in Ceramic Science and Engineering in 1992 and has been at ORNL since 1994. Dr. Pint is the principal investigator for numerous R&D projects including corrosion issues in fossil energy, nuclear energy, fusion energy and combined heat and power systems. His research covers compatibility, lifetime predictions, environmental effects and coatings in all types of power generation. In 2014, he was named a Fellow of NACE International and ASM International.

James Keiser is a Distinguished Research and Development Staff Member and has worked in ORNL's Corrosion Science & Technology Group since 1974 where he has studied the compatibility of materials with the environments of energy producing systems. Studies have addressed the performance of metallic and ceramic materials in environments containing gaseous, liquid and supercritical corrodents. Several of his current projects concern corrosion issues in biomass liquefaction and gasification. Dr. Keiser received his B.S. in Materials Science and Ph.D. in Metallurgical Engineering and is a Fellow of NACE International and ASM International.

ABSTRACT

In both open and closed supercritical CO_2 (sCO_2) cycles, there is considerable interest in increasing the size and efficiency of such systems, perhaps by increasing the peak temperature. The current project is evaluating a wide range of Fe- and Ni-base alloys, which typically form protective Cr- and Al-rich surface oxides, and other candidate materials, including ceramics, with a goal of establishing maximum use temperatures in sCO_2 for each class of materials. A new sCO_2 system has been designed and built with up to 930°C (1700°F) and 55 MPa (8,000 psi) capabilities. Initial 500h experiments have been completed at 650°, 700° and 750°C with 20MPa CO_2. As has been observed in other studies, higher alloyed Fe- and Ni-base alloys show protective behavior, relatively unaffected by the sCO_2 environment, while lower alloyed Fe-base alloys were more severely attacked. With increasing temperature, mass gains were slightly higher for the M-Cr alloys that formed protective chromia scales but some alumina-forming alloys had the highest mass gain at 650°C. Comparisons in 1 bar dry air and CO_2 with and without O_2 and H_2O impurities were performed at 700°C as a baseline for the sCO_2 results.

INTRODUCTION

A wide range of open and closed Brayton and Rankine cycle systems employing supercritical CO_2 (sCO_2) as the working fluid have been proposed for power generation applications [e.g. Dostal 2006, Zhang 2006, Chen 2010, Iverson 2013, Wright 2013]. The highest temperature systems, 500°-760°C (930°-1400°F) at 20-30 MPa (2900-4350 psig, 200-300 bar) develop hot gas path environments that present challenging requirements of strength and environmental resistance for the materials of construction. At these temperatures and pressures, the number of candidate alloys is extremely limited. The open cycle system (i.e. Allam cycle [Allam, 2011, 2013a, 2013b] burns fossil fuels and captures CO_2 with 700°-775°C (1300°-

1430°F) sCO_2 turbine exhaust temperatures and 1150°C/300 bar (2100°F/4350 psig) combustor conditions. A thermal protection system such as a ceramic thermal barrier coating [Darolia 2013] will be needed to lower the metal temperature from 1150°C to ~900°C, as no conventional structural materials can realistically operate at those peak conditions for the extended lifetimes typically required of power generation systems [Pint 2006].

While CO_2 is sometimes described as inert, the available literature on the effects of CO_2 on high temperature oxidation suggests this is an unusual use of this term. Decades old work at 1bar CO_2 [McCoy 1965] suggested that internal carburization is an issue for conventional stainless steels that normally form a protective Cr-rich external oxide or scale. More recent work has shown thick Fe-rich oxides formed on ferritic-martensitic (9-12%Cr) steels exposed to sCO_2 at 550°C [Rouillard 2011] that would normally form a thin protective scale at those temperatures. For Ni-base alloys, there is similar concern that strengthening elements that readily form carbides (e.g. W, Ta, Ti) could be internally carburized by a similar mechanism. Several groups have investigated high temperature sCO_2 compatibility over a wide range of materials [Oh 2006, Dunlevy, 2009, Tan 2011, Moore, 2012, Firouzdor 2013, He 2014].

The current project at Oak Ridge National Laboratory (ORNL) was initiated to provide a broad materials assessment of the sCO_2 compatibility of relevant Fe- and Ni-base alloys with evaluations up to 760°C/30MPa (1400°F/4500psig). A new experimental rig was developed with those capabilities and the first 500h results at 650°-750°C are reported here along with 1 bar results at 700°C to provide a baseline for comparison.

EXPERIMENTAL PROCEDURE

The sCO_2 system at ORNL utilizes an autoclave fabricated from Haynes International alloy 282, a γ'-strengthened superalloy intended for high temperature structural applications. The use of this alloy gives the system a capability for operation at pressures (55 MPa, 8,000 psi) and temperatures (927°C, 1700°F) in excess of those that can be achieved by other systems used for high temperature sCO_2 studies. The autoclave is operated in a vertical orientation inside a three-zone furnace, Figure 1. The internal dimensions of the autoclave are ~266 mm (10.5 in.) x 83 mm (3.25 in.) so that it can hold a considerable number of samples, typically mounted on an alloy 282 sample rack that sits on the bottom of the autoclave, Figure 1. The specimens were held on alumina rods with alumina spacers between specimens. The supercritical fluid was continuously fed into the autoclave through a supply tube that extended to within a few mm of the

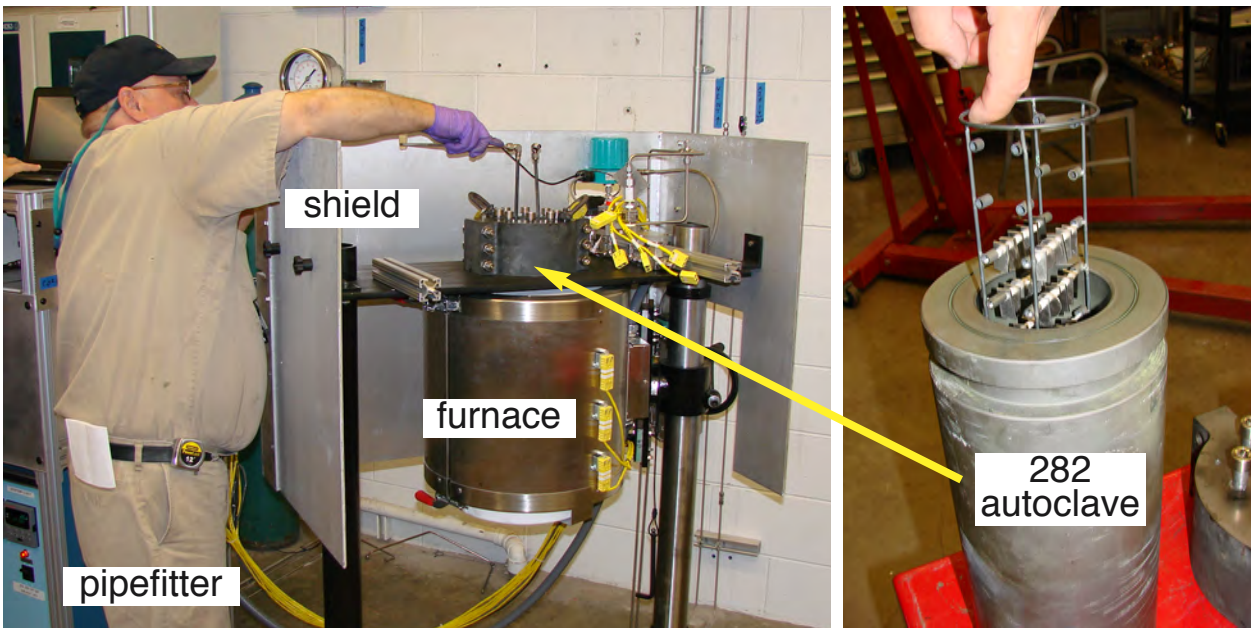

Figure 1. ORNL sCO_2 rig

bottom of the autoclave. The fluid was supplied by a Supercritical 24 constant flow dual piston pump, which permitted the feed rate to be controlled in the range of 0.01– 24.0 mL/min with 1.0 mL/min used for these experiments. The pressure in the system was controlled by use of a backpressure control valve which adjusted the orifice size as part of a feedback loop whose signal was based on the output of a pressure transducer located between the autoclave and the control valve. To prevent an inadvertent overpressurization of the system, a rupture disc and a pressure relief valve were built into the same high-pressure line between the autoclave and the control valve. For these 500 h experiments, liquid CO_2 was provided from a cylinder containing CO_2 with a purity of at least 99.995%. The specifications of the CO_2 called for <5 ppm moisture and <5 ppm total hydrocarbons. The specimens were slowly heated to temperature over several hours, held for 500 h (with ±10°C variation across the autoclave) and then slowly cooled to room temperature. The materials used in these experiments are listed in Table 1 along with their measured compositions. Coupons were typically 1.5 mm thick and 1 x 2 cm with a final 600 grit surface finish on all sides. The specimens were ultrasonically cleaned in acetone and methanol prior to exposure. Mass change was measured on a Mettler Toledo model XP205 balance (±0.04 mg accuracy or ±0.01

Table 1. Chemical composition of the alloys measured by inductively coupled plasma and combustion analyses in mass%.

Alloy	Fe	Ni	Cr	Al	Other
Ferritic chromia-forming steels					
Gr.91	89.7	0.1	8.3	<	1Mo,0.3Mn,0.1Si
Save12	83.4	0.3	9.6	0.01	2.6Co,3W,0.4Mn,0.1Si
410SS	86.9	0.1	11.8	0.04	0.5Mn,0.4Si
EBrite	72.6	0.1	25.8	<	1.0Mo,0.2Si,0.1V
AL294C	66.1	0.2	28.6	0.07	3.7Mo,0.2Mn,0.3Si,0.4Ti,0.3Nb
Austenitic Fe-base chromia-forming steels					
201SS	70.8	4.1	16.2	<	6.7Mn,0.9Cu,0.3Mo,0.5Si,0.2Co
347HFG	66.0	11.8	18.6	0.01	1.5Mn,0.8Nb,0.4Si,0.2Mo,0.2Co
304H+SP	70.4	8.4	18.4	<	1.6Mn,0.3Mo,0.4Cu,0.3Si
310HCbN	51.3	20.3	25.5	<	0.3Co,0.4Nb,1.2Mn,0.3Si,0.3N
NF709	49.0	25.0	22.3	0.02	1.5Mo,0.2Nb,1.0Mn,0.4Si
800H	43.2	33.8	19.7	0.7	1.0Mn,0.3Si,0.5Ti,0.3Cu
HR120	35.0	37.6	24.7	0.1	0.7Mn,0.6Nb,0.3Mo,0.2Si
Fe-base alumina-forming alloys					
AFA OC4	49.1	25.2	13.9	3.5	2.5Nb,2W,1.9Mn,2Mo,0.5Cu,0.2Si
Ohm40	81.7	0.5	12.7	3.6	0.4Mn,0.3Ti,0.2Si,0.1V
APMT	69.2	0.2	21.1	5.0	0.2Hf,0.1Mn,2.8Mo,0.6Si,0.3Y,0.1Zr
PM2000	74.1	0.02	19.1	5.5	0.5Ti,0.4Y,0.25O
Ni-base chromia-forming alloys					
IN718	18.8	52.8	18.2	0.6	5Nb,3Mo,1Ti,0.3Mn,0.1Si
Hastelloy X	17.9	46.8	22.1	0.09	9.5Mo,1.8Co,0.6W,0.3Si,0.7Mn
IN625	4.0	60.6	21.7	0.09	9.4Mo,3.6Nb,0.2Ti,0.2Si,0.1Mn
HR230	1.5	60.5	22.6	0.3	12.3W,1.4Mo,0.5Mn,0.4Si
CCA617	0.6	55.9	21.6	1.3	11.3Co,8.6Mo,0.4Ti,0.1Si
HR282	0.2	58.0	19.3	1.5	10.3Co,8.3Mo,0.06Si,2.2Ti,0.1Mn
IN740	1.9	48.2	23.4	0.8	20.2Co,2.1Nb,2.0Ti,0.3Mn,0.5Si
Ni-base alumina-forming alloys					
HR224	27.2	47.0	20.3	3.8	0.3Co,0.34Mn,0.39Si,0.37Ti
HR214	3.5	75.9	15.6	4.3	0.2Mn,0.1Si,0.02Zr
NM105	0.8	53.0	15.5	4.9	19.0Co,4.7Mo,1.4Ti,0.1Mn,0.1Si,0.1Zr
713LC	0.03	74.2	12.1	6.2	4.5Mo,2.1Nb,0.7Ti,0.06Zr
CM247	0.07	59.5	8.5	5.7	9.8Co,9.9W,0.7Mo,3.1Ta,1.0Ti,1.4Hf
PWA1483	0.03	60.6	12.0	3.4	8.8Co,5.2Ta,4.0Ti,4.1W,1.9Mo
NiCrAlYHf	0.01	72.2	15.5	12.0	0.14Hf,0.05Y
Ceramic					
CVD SiC	<	0.01	<	<	69.8Si,30.2C,0.003O

< indicates less than 0.01%

mg/cm^2). Similar specimens were exposed at 1 bar in a horizontal alumina tube with end caps within a 3-zone furnace for better temperature control. Under these conditions, 500 h experiments were conducted at 700°C, in dry air, high-purity CO_2, CO_2 with 0.15%O_2 and a mixed CO_2+10vol.%H_2O with 10 specimens (bold in Table 1) in each test held in an alumina boat. After exposure, specimens were Cu-plated to protect the surface oxide and metallographically mounted and imaged with light microscopy.

RESULTS

Figures 2-7 summarize the mass change data from the 7 conditions studied. In the 1 bar experiments, only the 10 alloys shown in Figure 2 were exposed. These alloys were selected to represent the major alloy classes denoted in Table 1, Fe- and Ni-base alloys that form chromia and alumina scales. For most of the alloys, the mass gains were small suggesting protective scale formation under these conditions and only minor effects of the CO_2 environment after these 500 h exposures. In general, the chromia-forming alloys (310H, 230, 740, 282) showed slightly higher mass gains after 700° and 750°C in 200 bar CO_2 compared to 650°C, as would be expected with the higher temperatures. The alloy 282 specimen exhibited a higher mass gain after the 750°C sCO_2 exposure, Figure 2. In two cases mass losses were observed: the ferritic steel E-Brite specimen at 700°C in 200 bar CO_2 and the austenitic steel 347HFG specimen in CO_2-10%H_2O. High mass gains were exhibited for the lowest alloyed material, Gr.91 steel and occasionally for 347HFG. The mass gains for Gr.91 are somewhat unreliable as the thick oxides can spall on cooling due to the strain energy associated with the CTE mismatch between the alloy and oxide.

Figure 3 summarizes the mass change data for the ~30 specimens exposed at 650°, 700° and 750°C in 200 bar CO_2 as a function of their Cr content. Again, the majority of specimens showed a low mass change and only the lowest-alloyed Fe-base alloy specimens exhibited high mass gains suggesting the rapid formation of FeO_X under these conditions. As was noted above, when a thick oxide formed, the exact value of the mass gain is unreliable as the oxide is likely to spall. The CVD SiC specimen exhibited little or no mass change at these temperatures after 500 h. Two trends are noted between the temperatures (1) some alloys that had higher mass gains at 650°C (e.g. 410SS, AFA) showed less mass gain at 700° and 750°C; this can be attributed to faster Cr or Al diffusion in the substrate at the higher temperature enabling the

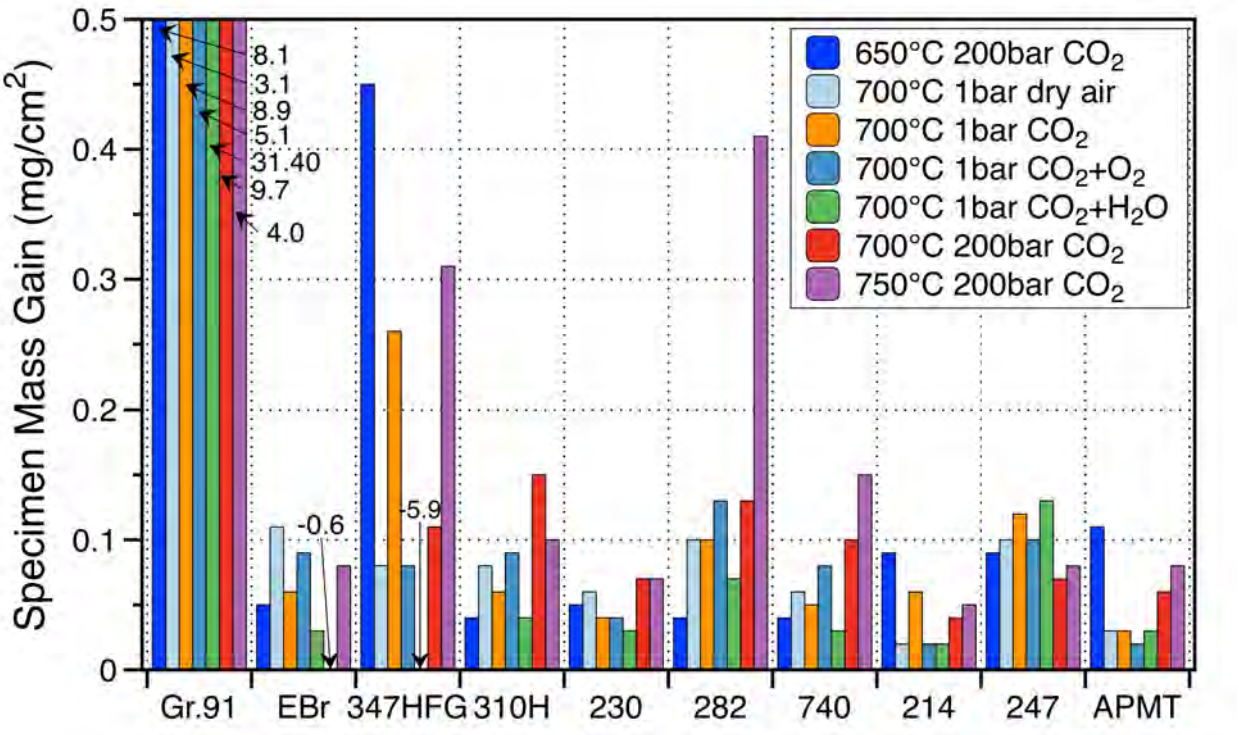

Figure 2. Mass change after 500h in each condition evaluated for 10 representative alloys

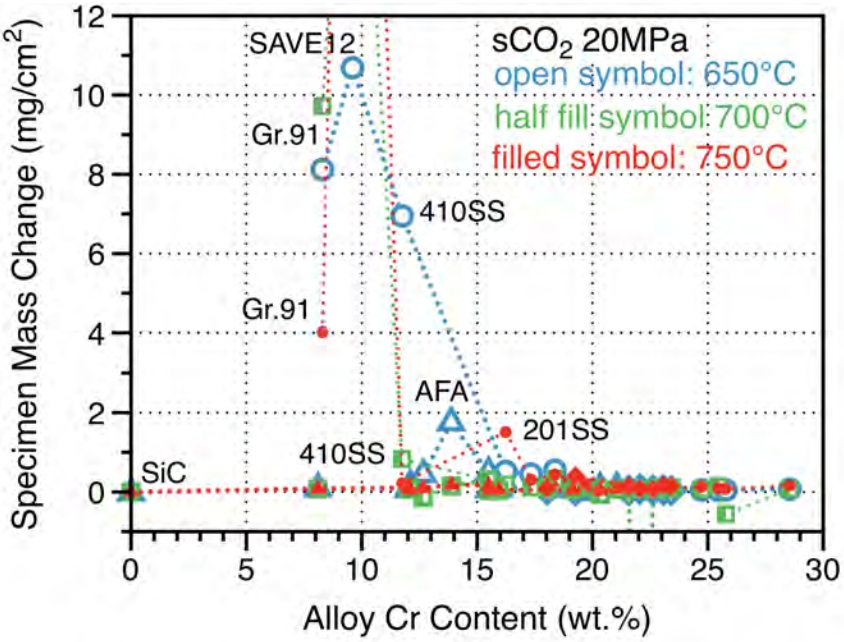

Figure 3. Specimen mass change as a function of alloy Cr content after 500h exposures in 200 bar CO_2 at 650° (open), 700°C (half-filled) and 750°C (filled symbols).

formation of a protective scale and (2) several alloys experienced a mass loss at 700°C whereas no mass losses were noted at 650° or 750°C. Further characterization is needed to explain the 2nd trend.

Figures 4-6 expand the y-axis of Figure 3 for the 650°-750°C data, respectively, in order to observe the behavior of the more highly-alloyed materials. The conventional austenitic (347HFG, 304H) and high Mn (201) stainless steels exhibited higher mass gains at 650°C compared to higher alloyed stainless steels

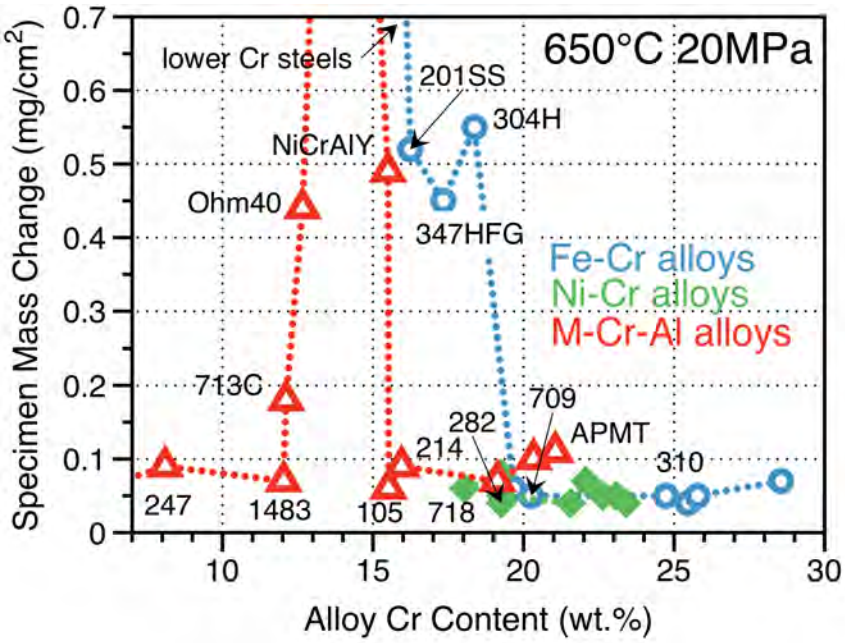

Figure 4. Specimen mass change as a function of alloy Cr content after a 500h exposure in 200 bar CO_2 at 650°C (1200°F): Fe-Cr alloys (circle), Ni-Cr (diamonds), M-Cr-Al (triangles).

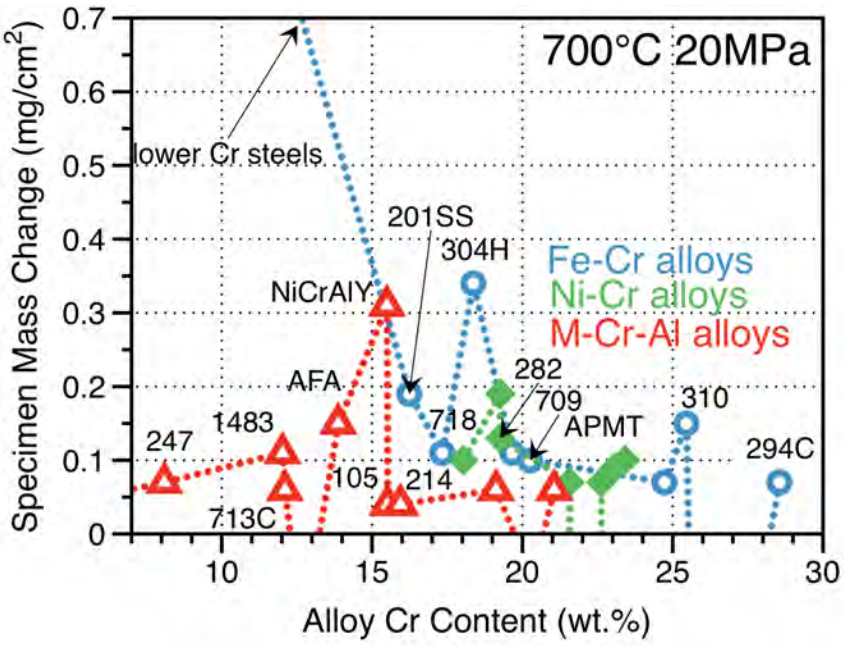

Figure 5. Specimen mass change as a function of alloy Cr content after a 500h exposures in 200 bar CO_2 at 700°C (1300°F): Fe-Cr alloys (circle), Ni-Cr (diamonds), M-Cr-Al (triangles).

such as NF709 and type 310, Figure 4. All of the chromia-forming Ni-base alloys performed similarly at 650°C with very low mass gains. Most of the alumina-forming alloys had higher mass gains than the chromia-forming Ni-Cr alloys and several had much higher mass gains. The AFA specimen as well as the "lean" FeCrAl, Ohmalloy 40, and a cast model superalloy bond coating alloy, NiCrAlYHf, all showed much higher mass gains, suggesting somewhat non-protective behavior.

In Figures 5 and 6, most of the Ni-Cr alloys performed similarly with relatively low mass gains. Figure 7 compares just the Ni-Cr alloys at 650°-750°C. While all of these alloys appeared to form a protective Cr-

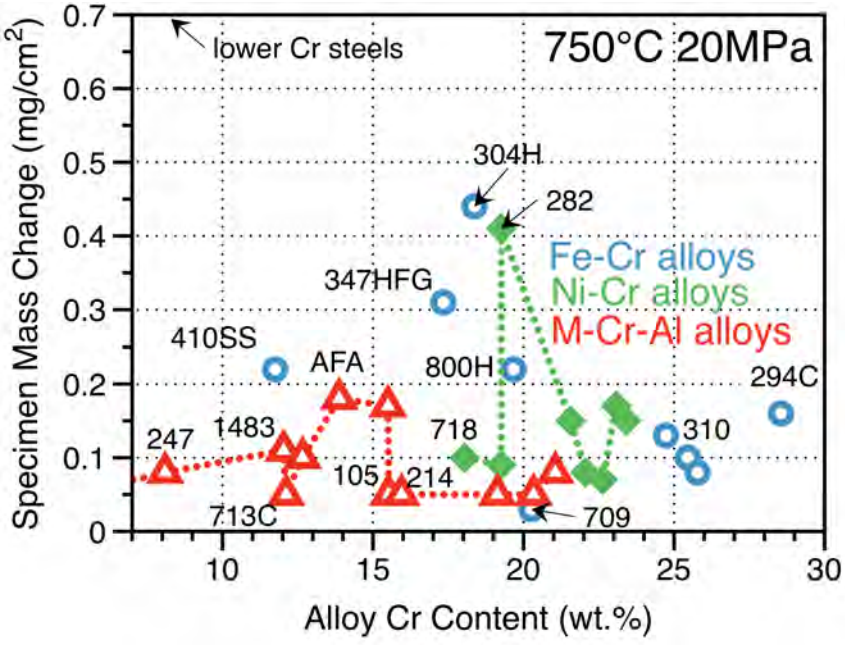

Figure 6. Specimen mass change as a function of alloy Cr content after a 500h exposures in 200 bar CO_2 at 750°C (1380°F): Fe-Cr alloys (circle), Ni-Cr (diamonds), M-Cr-Al (triangles).

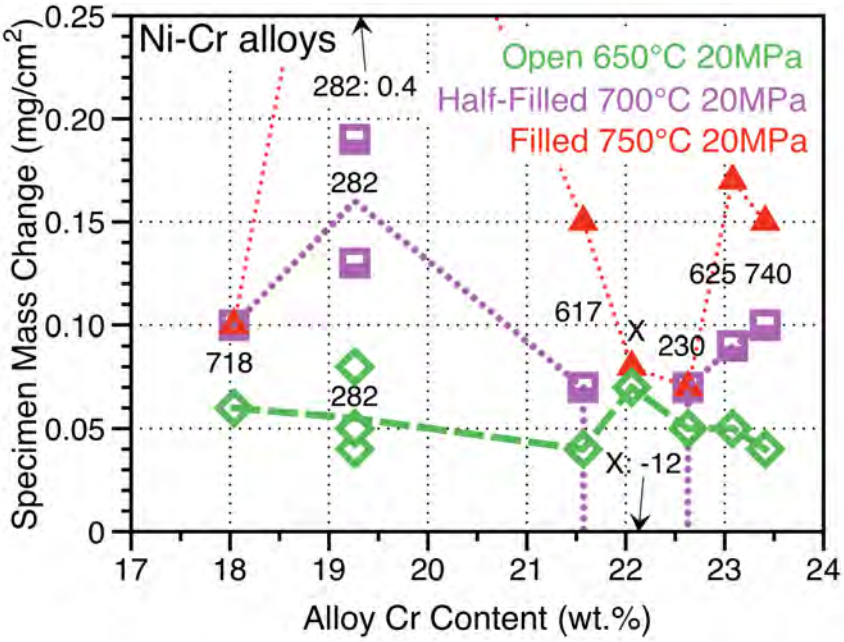

Figure 7. Specimen mass change as a function of alloy Cr content for Ni-base alloys after 500h exposures in 200 bar CO_2 at 650°-750°C (1200°-1380°F).

rich oxide, it is not surprising that the mass gain increased as the temperature increased. The two exceptions were the mass loss observed for alloy X specimen at 700°C and the higher mass gain for the alloy 282 specimen at 750°C (neither specimen has been characterized at this time to determine the reason for this behavior). In contrast to the Ni-Cr alloys, many of the alumina-forming alloys exhibited lower mass gains at 700° and 750°C (compare Figures 4-6). Typically, alumina-forming alloys are selected for applications above 900°C (1650°F) where their slower oxidation kinetics are more significant for long-term component lifetime. At 650°C, many alumina-forming alloys with only 3-5% Al have difficulty forming an alumina scale because of the slow reaction kinetics to form alumina and the relatively slow Al diffusion in the substrate, which inhibits selective oxidation of Al to form alumina. However, as the temperature increased thereby increasing oxidation and Al diffusion (in the alloy) rates, alumina formation was easier [Pint 1999]. Another aspect in Figure 5 is that the dashed lines note that several alloys exhibited mass losses at 700°C: X, E-Brite, Ohmalloy 40 and 224. Characterization of these specimens is in progress to explain this selective behavior. In Figure 6, the dashed line was removed for the Fe-Cr alloys because of the range of behavior, such as the higher mass gain of the high Mn type 201 stainless steel specimen. It should be noted that the low mass gains for some of the alloys (410SS, 347HFG, 304H) at 750°C could be an indication of more protective behavior or a net result of a thicker scale with some spallation. Further characterization is needed to understand these most recent results. Furthermore, these promising results may be related to the 500h exposure time. Longer exposures are needed to verify that these materials remain compatible.

Examples of the initial microstructural characterization are shown in Figures 8-13. Figure 8 shows cross-sections from Gr.91 at several conditions. Prior work had exposed a specimen of this alloy for 5,000 h (10, 500-h cycles) at 650°C in laboratory air. Figure 8c shows that a thin protective scale was formed on a majority of the surface after this extended exposure. In contrast, after only 500 h at 700°C in dry air, Gr.91 formed a thick, duplex oxide that is typical of Fe-based alloys that are unable to form a protective Cr-rich oxide, Figure 8d. A duplex oxide is formed in many environments (air, steam, liquid metals, CO_2, etc.) and its hallmark is an outer Fe-rich oxide, typically free of Cr and either Fe_3O_4 or Fe_2O_3 depending on the oxygen partial pressure; and an inner Cr-rich oxide layer that may contain unoxidized metal precipitates [Otsuka, 1989]. The Gr.91 exposures in CO_2 suggest that it is particularly attacked by the presence of 200 bar CO_2 both at 650°C (Figure 8a) and 700°C (Figure 8b). In 1 bar CO_2 at 700°C, the thick oxide was not continuous

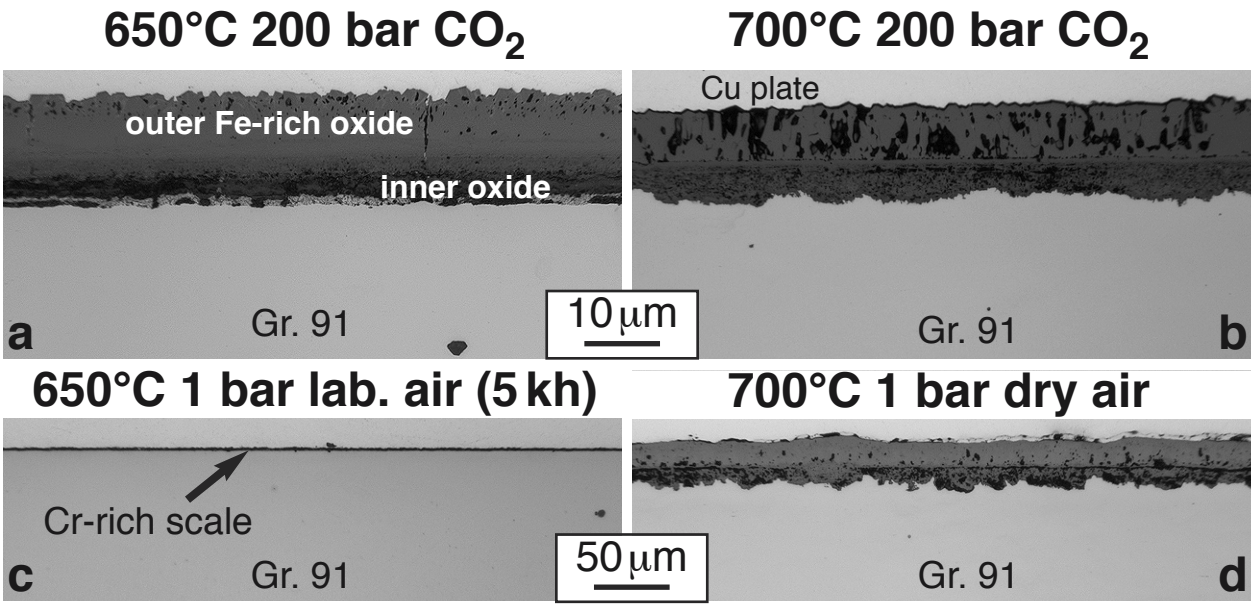

Figure 8. Light microscopy of polished cross-sections of Grade 91 ferritic-martensitic steel after (a) 500h at 650°C in 200 bar CO_2 (b) 500h at 700°C in 200 bar CO_2, (c) 5,000h at 650°C in laboratory air and (d) 500h at 700°C in 1 bar dry air.

on the surface and some regions were able to retain a protective scale after 500h. However, what begins as oxide nodules with a duplex structure, grows laterally leading to a complete coverage of the thick oxide after longer times. In 200 bar CO_2, the duplex oxide was continuous, Figure 8b. One previously suggested explanation for this breakdown is that internal carburization of Cr in the presence of CO_2 prevents Cr from participating in the formation of a protective Cr-rich oxide [Quadakkers 2011]. Pressure, temperature and environment may affect the structure of the duplex scale and further characterization of these thick oxides is required.

Similar reaction products were sometimes observed for 347HFG in Figure 9. In this case, protective behavior, i.e. a thin Cr-rich oxide, was observed at 700°C in dry air, Figure 9c, but thick duplex oxide nodules began to form at 700°C in 1 bar CO_2, Figure 9d. At higher magnification of the same specimen in Figure 9e, the duplex oxide structure appeared somewhat different in CO_2 at 700°C/1 bar compared to 650°C/200 bar in Figure 9a. However, nodule formation was not observed after exposure in 200bar CO_2 at 700°C.

For the higher alloyed chromia-forming alloys, Figure 10 shows examples of two of the alloys, 310HCbN stainless steel and Ni-base alloy 740, that exhibited low mass gains in the presence of 200 bar CO_2 at 650°C (Figures 10a and 10c) and 700°C (Figure 10b and 10d). A thin, Cr-rich scale was observed in all cases, with only an occasional oxide nodule observed. After the 700°C exposure, the oxide scale appeared somewhat thicker than was observed at 650°C. Similar oxides were observed in the other 700°C conditions but not shown here.

As suggested by the mass gain data in Figures 1, 4 and 5, Figure 11 shows examples for alloy APMT where an alumina-forming alloy formed a thinner scale at the higher temperature. Similar observations were apparent for alloy 214, a Ni-base alumina-forming alloy, Table 1. A more complicated reaction product was observed for alloy 247, Figure 12. This DS superalloy was specifically included because of its high Hf content. The light microscopy suggested some internal oxidation, perhaps associated with the Hf-rich precipitates in the alloy, which appear to have been internally oxidized in all of the environments (including dry air at 700°C) whenever the precipitates were at or near the reaction interface.

Finally, Figure 13 shows two unique specimens exposed to 200 bar CO_2 at 650°C. Figure 13a shows the reaction product formed on cast NiCrAlYHf. Rather than the protective alumina scale that forms on this alloy at 1000°-1150°C (1800°-2100°F) [Unocic 2013], this specimen formed a thick reaction product with

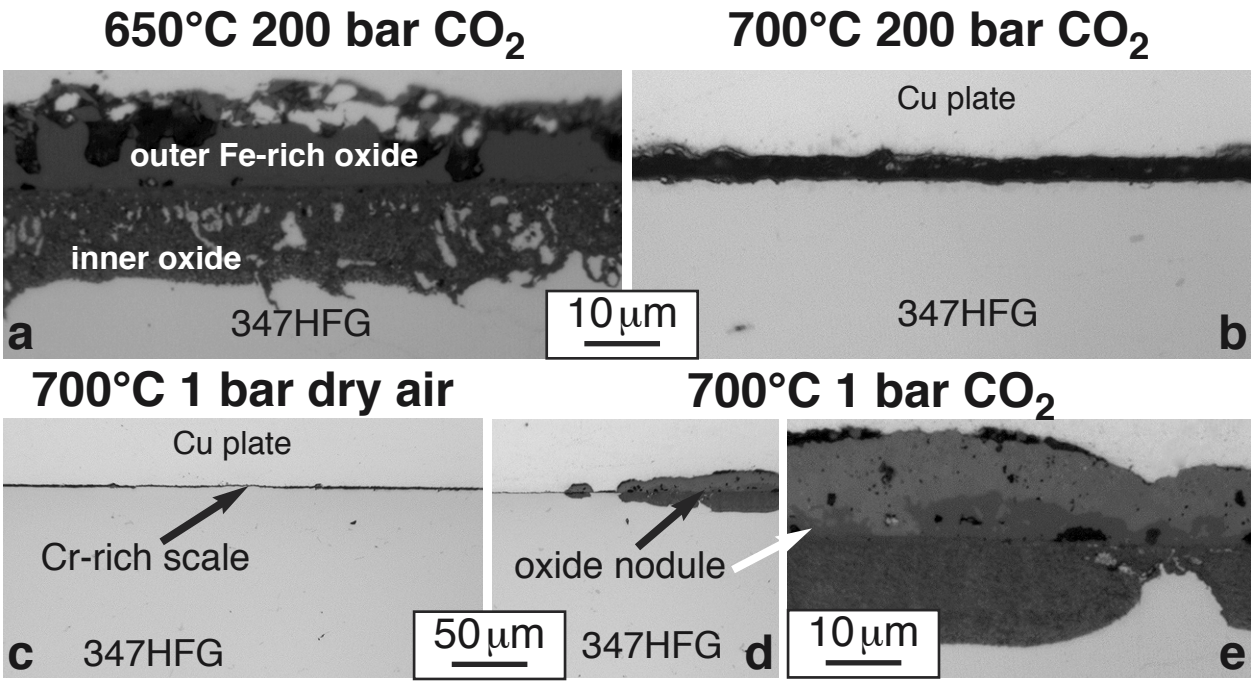

Figure 9. Light microscopy of polished cross-sections of type 347HFG stainless steel after 500 h at (a) 650°C in 200 bar CO_2, (b) 700°C in 200 bar CO_2 , (c) 700°C in 1 bar dry air and (d,e) 700°C in 1 bar CO_2 (two magnifications).

internal oxidation in the presence of sCO_2 at 650°C. Figure 13b shows the shot peened ID of a 304H tube specimen. While shot peening has been effective on the steamside of stainless steel tubes in commercial coal-fired boilers [Pint 2012] and in laboratory testing in steam at 620°C (1150°F) [Tossey, 2011] and 650°C (1200°F) [Pint 2014a], it did not appear to be effective in the presence of sCO_2 at 650°C where a non-protective duplex scale formed on the shot-peened ID. As suggested by the mass change data, both alloys performed better at higher temperatures.

DISCUSSION

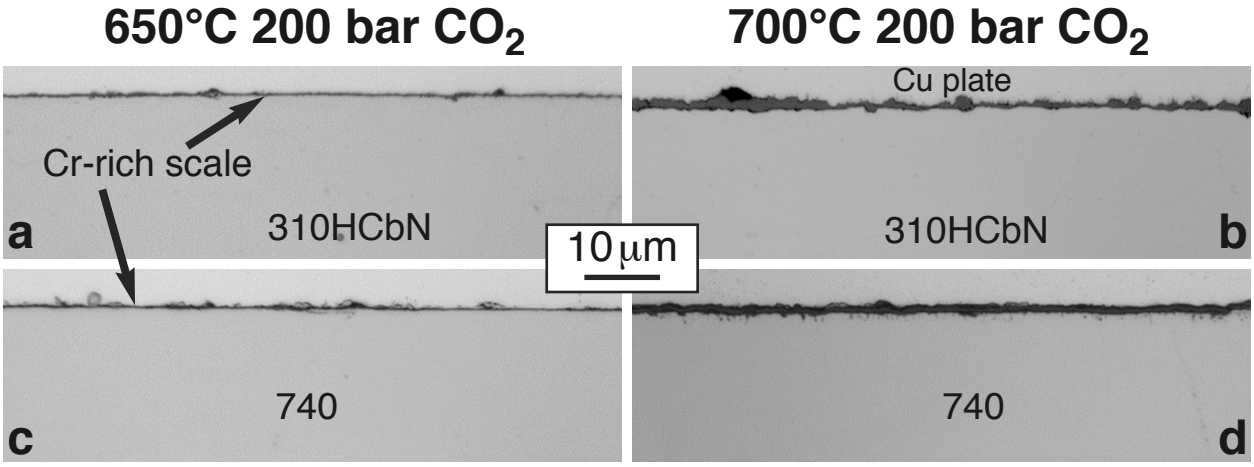

Figure 10. Light microscopy of polished cross-sections of alloys 310 (a,b) and 740 (c,d) after 500 h at (a,c) 650°C in 200 bar CO_2 and (b,d) 700°C in 200 bar CO_2.

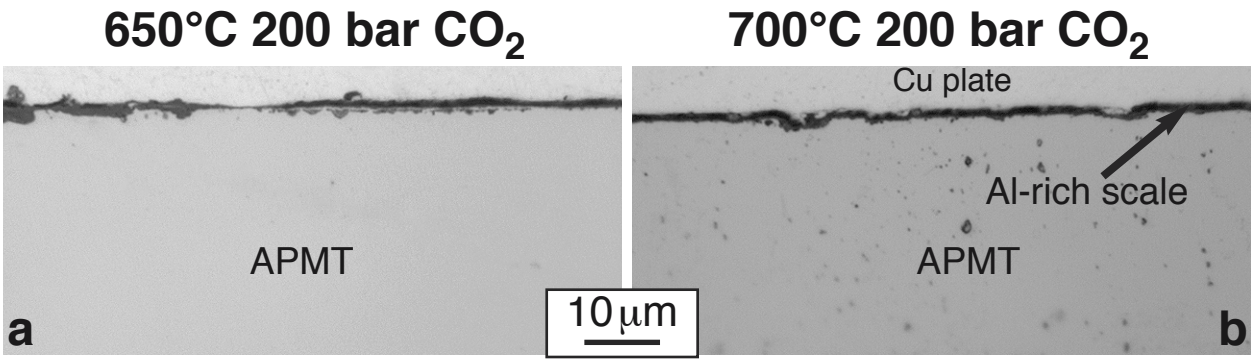

Figure 11. Light microscopy of polished cross-sections of FeCrAl alloy APMT after 500 h at (a) 650°C in 200 bar CO_2 and (b) 700°C in 200 bar CO_2.

Initial results are presented from the new ORNL sCO_2 test rig. Future work will continue this 500 h experiment series to different temperatures as needed and vary the pressure from 12.5-30 MPa (1800-4350 psi). These conditions were selected in order to repeat prior conditions covered by other research groups at MIT and Wisconsin, while expanding to higher pressures at 750°C than have previously been explored. The current results with thick reaction products for low-alloyed stainless steels are consistent with prior observations [e.g. Rouillard 2011]. Similar observations with thin reaction products for higher-alloyed materials, also have been observed previously [e.g. Dunlevy, 2009].

For the present results, more characterization is needed, such as electron probe microanalysis, in order to better understand the various reaction products. Based only on the mass change data, the effect of CO_2 pressure appears minimal at 700°C (1 vs. 200 bar), Figure 2. One of the key mechanistic issues to be further explored is the ingress of C through the external scale and whether pressure affects this mechanism. While the carbon activity in the gas is low in these environments (10^{-44} at 700°C in 1bar CO_2), McCoy [1965] and others have seen examples of internal carburization. The most likely explanation for the internal attack is that C penetrates the scale and its activity increases at the low O activity at the metal-scale interface where Cr/Cr_2O_3 or Al/Al_2O_3 equilibrium exists. The traditional view has been that alumina scales are less permeable to C than chromia scales (with the opposite true for N_2) [Jönsson 1997]. Thus, at some high temperature sCO_2 conditions, alumina-forming alloys may be the primary candidates. However, for high pressures at 700°-750°C, precipitation strengthened Ni-base superalloys like 740 [Zhao 2003, Shingledecker 2013] and 282 [Pike 2008] are likely candidates with the former alloy recently gaining ASME boiler and pressure vessel code qualification and a similar code case starting for alloy 282 in 2015.

For the high combustion temperatures 1100°-1150°C (2000°-2100°F) envisioned for the open Allam cycle [Allam 2013a], even the most oxidation resistant alloys will likely require protective coatings. In air- and

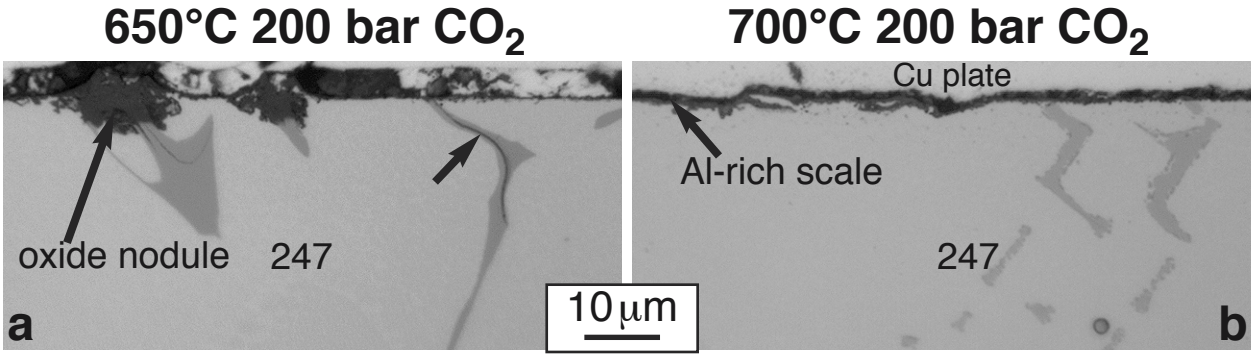

Figure 12. Light microscopy of polished cross-sections of Ni-base superalloy 247 after 500 h at (a) 650°C in 200 bar CO_2 and (b) 700°C in 200 bar CO_2. Arrow in (a) marks an apparent crack.

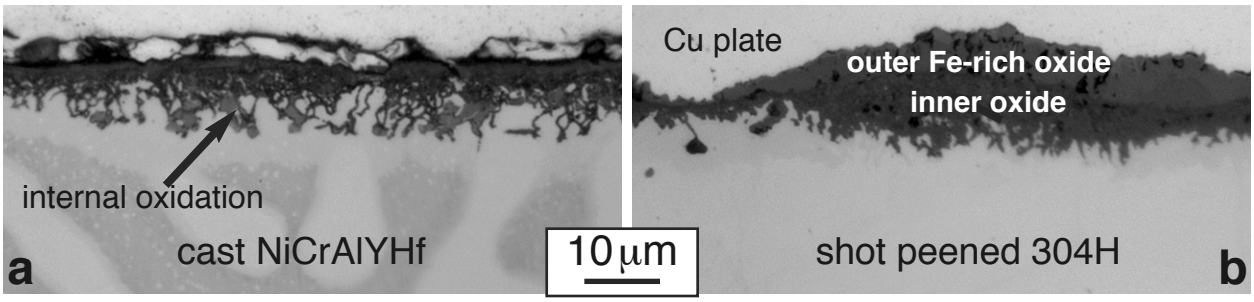

Figure 13. Light microscopy of polished cross-sections after 500 h at 650°C in 200 bar CO_2 (a) cast NiCrAlYHf and (b) shot peened ID of a 304H tube.

land-based turbines, the highest performance alumina-forming single-crystal superalloys (e.g. 1483) are coated with alumina-forming metallic coatings (like the cast, model NiCrAlYHf specimens) to increase durability and low thermal conductivity ceramic top coatings (e.g. Y_2O_3-stabilized ZrO_2) are used to lower the metal temperature. For aero-engines, metal temperatures may reach 1100°-1150°C (2000°-2100°F) during takeoff and landing for ~5-10% of ~15,000 h commercial engine wing time but the majority of operation is at hundreds of degrees lower temperature. To achieve continuous 1150°C gas temperature, a TBC will be required to significantly lower the metal temperature. Essentially, the coating is then life limited by interdiffusion between the Al-rich coating and the substrate. Initial ORNL work on TBC lifetime in 1bar 90%(CO_2-0.15O_2)-10%H_2O found no detrimental effect of this environment on TBC lifetime in furnace cyclign tests [Pint 2014b].

Future experiments will consider the effect of impurities in the CO_2 on the reaction kinetics. The initial 1 bar experiments with O_2 and H_2O additions are the first step in creating a baseline for those experiments. A more sophisticated pumping system will be required for controlled impurities in sCO_2 and construction of an experimental rig for creating controlled impurity exposures has been proposed for 2015. In addition, future experiments will include small (25mm, 1") tensile bars to evaluate (ex-situ) the effect of the sCO_2 environment on alloy mechanical properties. Obviously, much more work is needed to understand sCO_2 material compatibility for higher temperature/pressure conditions and longer lifetime applications needed for high efficiency power generation systems.

CONCLUSIONS

Initial sCO_2 results have been generated with 500 h exposures at 650°-750°C (1200°-1380°F) in 20 MPa (2900 psi) CO_2. A wide range of Fe- and Ni-base alloys, which form protective Cr- and Al-rich surface oxides, has been evaluated. Many of the higher alloyed materials and SiC exhibited low mass changes and thin reaction products at all three temperatures with expected thicker reaction products at 700° and 750°C. As has been observed in other studies, lower alloyed steels can form non-protective Fe-rich oxides in the presence of CO_2 when normally thin protective Cr-rich oxides from under other oxidizing conditions. Similarly, some alumina-forming alloys were not as protective at 650°C as at 700°-750°C likely because of the difficulty in selectively forming an alumina scale at the lower temperature. Baseline data at 1 bar acquired at 700°C for comparison suggested that many of these materials were relatively unaffected by the sCO_2 environment and that pressure (1 vs. 200 bar) had a minimal effect after 500 h of exposure. More characterization is in progress to understand the mass losses for a few specimens at 700°C and the mass change results presented at 750°C. Further evaluation of the reaction products formed under all of these conditions is needed.

NOMENCLATURE

AFA = alumina-forming austenitic steel (Grade OC4 investigated in this study)
APMT = Advanced Powder Metallurgy Tube (Sandvik/Kanthal FeCrAl alloy)
CTE = Coefficient of Thermal Expansion

CVD = Chemical Vapor Deposition
DS = Directionally Solidified (superalloy fabrication technique with aligned grain boundaries)
Gr. = Grade (steel)
HFG = H (high carbon) FG (fine grain structure)
ID = inner diameter of a tube
Ohm40 = Allegheny Ludlum alloy Ohmalloy 40
ORNL = Oak Ridge National Laboratory
TBC = Thermal Barrier Coating (consisting of a metallic bond coating and ceramic top coating)

REFERENCES

Allam, R. J., Palmer, M. R., Brown, Jr., G. W., 2011, "System and Method for High-Efficiency Power Generation Using a Carbon Dioxide Circulating Working Fluid," International Patent No. WO 2011/094294 A2, Aug. 4, 2011.

Allam, R. J., Palmer, M. R., Brown Jr., G. W., Fetvedt, J., Freed, D., Nomoto, H., Itoh, M., Okita, N., Jones Jr., C., 2013a, "High efficiency and low cost of electricity generation from fossil fuels while eliminating atmospheric emissions, including carbon dioxide," Energy Procedia 37, 1135–1149.

Allam, R. J., 2013b, "NET Power's CO_2 cycle: the breakthrough that CCS needs," Modern Power Systems, July 2013 (http://www.modernpowersystems.com/ features/featurenet-powers-co2-cycle-the-breakthrough-that-ccs-needs/)

Chen, H., Goswami, D. Y., Stefanakos, E. K., 2010, "A review of thermodynamic cycles and working fluids for the conversion of low-grade heat," Renewable & Sustainable Energy Reviews 14, 3059-3067.

Darolia, R., 2013, "Thermal barrier coatings technology: critical review, progress update, remaining challenges and prospects," International Materials Reviews 58(6), 315-348.

Dostal, V., Hejzlar, P., Driscoll, M. J., 2006, "The supercritical carbon dioxide power cycle: Comparison to other advanced power cycles," Nuclear Technology, 154(3), 283-301.

Dunlevy, M. W., 2009, "An Exploration of the Effect of Temperature on Different Alloys in Supercritical Carbon Dioxide Environment," M.Sc. Thesis, MIT, Cambridge, MA.

Firouzdor, V. Sridharan, K., Cao, G., Anderson, M. Allen, T. R., 2013, "Corrosion of a stainless steel and nickel-based alloys in high temperature supercritical carbon dioxide environment," Corrosion Science 69, 281-291.

He, L. F., Roman, P., Leng, B., Sridharan, K., Anderson, M. Allen, T. R., 2014, "Corrosion behavior of an alumina forming austenitic steel exposed to supercritical carbon dioxide," Corrosion Science 82, 67–76.

Iverson, B. D., Conboy, T. M., Pasch, J. J., Kruizenga, A. M., 2013, "Supercritical CO_2 Brayton cycles for solar-thermal energy," Applied Energy, 111, 957-970.

Jönsson, B., Svedberg, C., 1997, "Limiting Factors for Fe-Cr-Al and NiCr in Controlled Industrial Atmospheres," Mater. Sci. Forum, 251-254 (1997) 551-558.

McCoy, H. E., 1965, "Type 304 Stainless Steel vs Flowing CO_2 at Atmospheric Pressure and 1100-1800°F," Corr., 21, 84-94.

Moore, R., Conboy, T., 2012, "Metal Corrosion in a Supercritical Carbon Dioxide – Liquid Sodium Power Cycle," Sandia National Laboratory Report SAND2012-0184.

Oh, C. H., Lillo, T., Windes, W., Totemeier, T., Ward, B., Moore, R., Barner, R., 2006, "Development Of A Supercritical Carbon Dioxide Brayton Cycle: Improving VHTR Efficiency And Testing Material Compatibility," Idaho National Laboratory Report INL/EXT-06-01271.

Otsuka, N., Shida Y., Fujikawa, H., 1989, "Internal-External Transition for the Oxidation of Fe-Cr-Ni Austenitic Stainless Steels in Steam" *Oxidation of Metals* 32, 13-45.

Pike, L. M., 2008, "Development of a Fabricable Gamma-Prime (γ') Strengthened Superalloy," in *Superalloys*

2008, R. C. Reed et al. eds TMS, Warrendale, PA, 2008, p.191-200.

Pint, B. A., Leibowitz, J., DeVan, J. H., 1999, "The Effect of an Oxide Dispersion on the Critical Al content in Fe-Al Alloys," *Oxidation of Metals*, 51, 181-97.

Pint, B. A., DiStefano, J. R., Wright, I. G., 2006, "Oxidation Resistance: One Barrier to Moving Beyond Ni-Base Superalloys," Materials Science and Engineering A, 415, 255-263.

Pint, B. A., Shingledecker, J. P., Wright, I. G., 2012, "Characterization of Steam Oxidation Products from Field-Exposed Tubes," in *Advances in Condition and Remaining Life Assessment for Fossil Power Plants*, EPRI, Charlotte, NC, presented Hilton Head, SC, Oct. 2012.

Pint, B. A., Dryepondt, S., 2014a "Effects of Alloy Composition and Surface Engineering on Steam Oxidation Resistance," in Proc. 7th Inter. Conf. on Advances in Materials Technology for Fossil Power Plants, ASM International, Materials Park, OH presented Waikoloa, HI, Oct. 2013.

Pint, B. A., Unocic, K. A., Haynes J. A., 2014b "The Effect of Water Vapor Content and CO_2 on TBC Lifetime," in Proc. 7th Inter. Conf. on Advances in Materials Technology for Fossil Power Plants, ASM International, Materials Park, OH presented Waikoloa, HI, Oct. 2013.

Quadakkers, W. J., Olszewski, T., Piron-Abellan, J., Shemet, V., Singheiser, L., 2011, "Oxidation of Metallic Materials in Simulated CO_2/H_2O-rich Service Environments Relevant to an Oxyfuel Plant," Mater. Sci. Forum 696, 194-199.

Rouillard, F., Charton, F., Moine, G., 2011 "Corrosion Behavior of Different Metallic Materials in Supercritical Carbon Dioxide at 550°C and 250 bars," Corrosion 67(9), 095001

Shingledecker, J. P., Pharr, G. M., 2013, "Testing and Analysis of Full-Scale Creep-Rupture Experiments on Inconel Alloy 740 Cold-Formed Tubing," J. Mater. Eng. Performance, 22, 454-462.

Tan, L. Anderson, M., Taylor, D., Allen, T. R., 2011, "Corrosion of austenitic and ferritic-martensitic steels exposed to supercritical carbon dioxide," Corrosion Science 53, 3273-3280.

Tossey, B. M. Khan, H., Andress, T., 2011, "Steam Oxidation Resistance of Shot Peened Austenitic Stainless Steel Superheater Tubes," NACE Paper 11-186, Houston, TX, presented at NACE Corrosion 2011, Houston, TX, March 2011.

Unocic, K. A., Pint, B. A., 2013 "Oxidation Behavior of Co-Doped NiCrAl Alloys in Dry and Wet Air," *Surface and Coatings Technology*, 237, 8-15.

Wright, I. G., Pint, B. A., Shingledecker, J. P., Thimsen, D., 2013, "Materials Considerations for Supercritical CO_2 Turbine Cycles," ASME Paper #GT2013-94941, presented at the International Gas Turbine & Aeroengine Congress & Exhibition, San Antonio, TX, June, 3-7, 2013.

Zhang, X. R., Yamaguchi, H., Uneno, D., Fujima, K., Enomoto, M., Sawada, N. , 2006, "Analysis of a novel solar energy-powered Rankine cycle for combined power and heat generation using supercritical carbon dioxide," Renewable Energy, 31, 1839-1854.

Zhao, S. Q., Xie, X. S., Smith, G. D. Patel, S. J., 2003, "Microstructural stability and mechanical properties of a new nickel based superalloy," Mater. Sci. Eng. A 355, 96-105.

ACKNOWLEDGEMENTS

The experimental work at ORNL was conducted by M. Howell, M. Stephens and T. Jordan. Material was provided by Haynes International, Special Metals, Allegheny-Ludlum, Sumitomo Metals, Capstone Turbines, Sandvik (Kanthal), Siemens and Plansee. P. F. Tortorelli provided useful comments on the manuscript and calculated the C activity in CO_2. Research sponsored by the U. S. Department of Energy, Office of Fossil Energy, Coal and Power R&D.